Considerations of oblique impacts of non-spherical, graphite-epoxy projectiles

Joshua E. Miller[1,2]

[1] University of Texas at El Paso, 500 W. University Ave., El Paso, TX 79968, United States of America, jemiller2@utep.edu
[2] Jacobs, NASA Johnson Space Center, 2101 NASA Pkwy., Houston, TX 77058, United States of America, joshua.e.miller@nasa.gov

ABSTRACT

The DebriSat hypervelocity impact experiment, performed at the Arnold Engineering Development Center, is intended to update the catastrophic break-up models for modern satellites including many modern materials like structural panels of carbon-fiber, reinforced polymer (CFRP). Subsequent to the experiment, fragments of the DebrisSat have been extracted from porous, catcher panels, and thus far, one of the key observations from the collected fragments is that CFRP represents a large fraction of the fragments and that these fragments tend to be thin, flake-like structures or long, needle-like structures pointing to the need to consider non-spherical orbital debris. Previous work examined the case of an arbitrarily oriented cylindrical projectile impacting normal to the surface of a simple double-wall, Whipple shield, with a thermal blanket on the outer surface [1]. This work extends that development using numerical simulations to oblique impacts at a representative orbital speed of 7 km/s and addresses the complexities associated with that addition.

1 INTRODUCTION

The DebriSat hypervelocity impact experiment, performed at the Arnold Engineering Development Center, is intended to update the catastrophic break-up models for modern satellites [2]. To this end, the DebriSat was built with many modern materials including structural panels of carbon-fiber reinforced polymer (CFRP). Subsequent to the experiment, fragments of the DebriSat have been extracted from porous catcher panels that were used to gather the debris from the impact event [2]. Thus far, one of the key observations from the collected fragments is that CFRP fragments represent a large fraction of the collected debris and that these fragments tend to be thin, flake-like structures or long, needle-like structures; whereas, debris with nearly equal dimensions is less prevalent. As current ballistic-limit models for shields are generally based upon spherical impacting particles, the experiment has pointed to a missing component in the current approach to ballistic modeling that must be considered [1].

While numerous shield types are currently in use for impact mitigation from orbital debris and meteoroids, the double-wall or Whipple shield is among the most prevalent. This shield achieves a high level of ballistic performance for minimal weight because the stresses induced in a projectile during impact are far above the stresses the solid particle can withstand resulting in a break-up of the particle. In the double-wall approach, an empty volume between the two walls of the shield gives a space for the debris to expand resulting in a distributed impact on the second, shield-wall. Even with the increased performance of this design, the shield-wall reaches a limit, which is the ballistic-limit of the shield-system. Commonly, the ballistic-limit is characterized through experiment to a characteristic dimension of the projectile, which has largely been based on the diameter of a sphere.

Spheres have beneficial qualities for shield characterization as there is no angle-of-attack (AOA) dependence for the shape (i.e. a sphere looks the same regardless of the orientation of the projectile on impact). Spheres also have some ballistic benefits as they result in a relatively uniform stress-state across the projectile. Furthermore, the shock waves originating from the sphere push material in the first wall approximately radially, which improves the spread of material. It has been experimentally observed with aluminum particles that departing from spheres decreases all-aluminum, Whipple shield performance, at least, for particles without an AOA impacting normal to the surface [1].

Complicating these experimental observations is that the pure, all-metal, Whipple shield is less prevalent in deployment due to thermal considerations. The presence of thermal shielding materials are known to affect the performance of double-wall shields depending on the construction and the placement of the thermal blanket, thus thermal materials should be included in an analysis to be representative of actual spacecraft. NASA and other agencies have performed numerous experimental campaigns on flight configurations with thermal materials, and

among those, a Whipple shield with a thermal blanket attached to the front of the outer bumper has been selected for this numerical study. This shield has the material configuration shown in Fig. 1.

a) b)

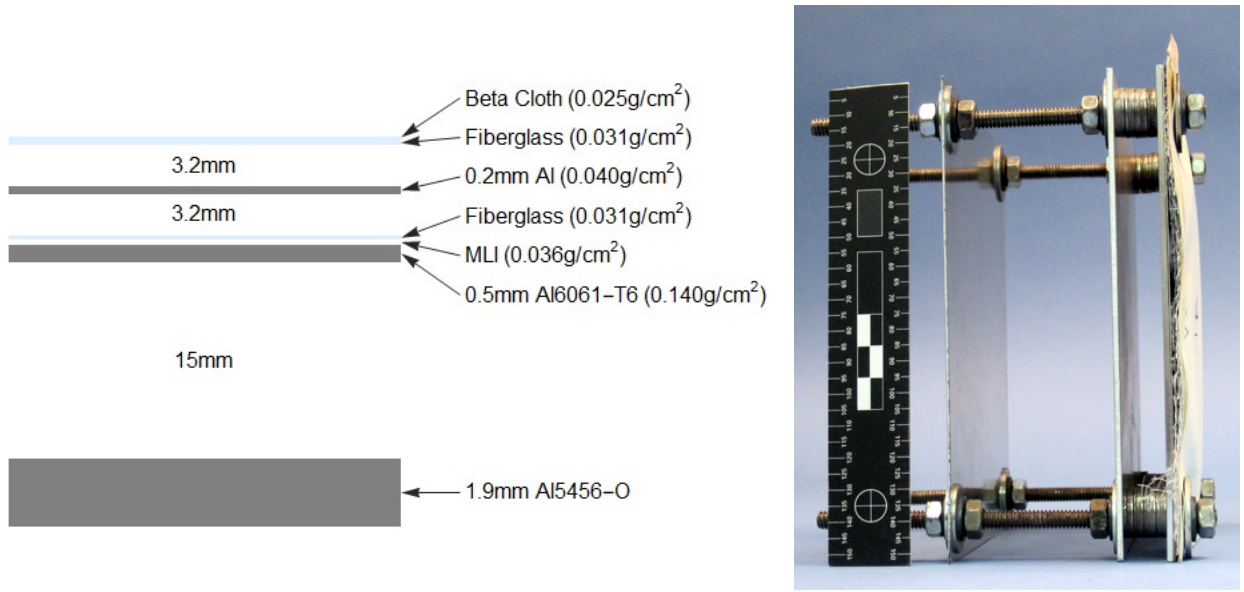

Fig. 1. Shield a) schematic for numerical simulation (layers scaled by mass; separations to scale) which represents b) a previously considered shield [1].

2 METHODS

This section documents the shield design considered in simulation, the numerical solution approach, and a comparison of validation simulations with obtained impact experiment results [4].

2.1 Shield description

The shield considered here is fundamentally an aluminum, Whipple shield; however, the shield also includes an enhanced, thermal-blanket over the top as shown in Fig. 1a. This shield is representative of an operational shield at the ISS, but has some subtle differences based on material model availability. The outermost aluminum wall, the "bumper", is made of 0.5 mm Al6061-T6, and the rear wall is made of a 1.9 mm Al5456-0. The two walls are separated from each other by 15 mm. Over the top of the outer wall is the enhanced, thermal-blanket. The outermost material is a combined Beta cloth and fiberglass layer that weighs 0.056 g/cm^2. Beyond those materials is an enhancement intended to boost protection from meteoroids and orbital debris (MMOD), which includes a bent 0.2 mm thick aluminum plate weighing 0.040 g/cm^2. The plate that separates the layers of 0.031 g/cm^2 fiberglass cloth is bent in opposite directions on each side by 3.2 mm [4]. Beneath the MMOD enhancement is a 0.036 g/cm^2 multilayer insulation (MLI) blanket. The total mass of the enhanced, thermal-blanket is 0.163 g/cm^2.

Fig. 1b is an image of the actual experimental article with a millimeter scale reference considered from a previous study [4]. In the experiments, a projectile impacts the target setup from the right. The schematic in Fig. 1a is of the two, right-most walls in Fig. 1b. The left-most plate is an article structural witness and is not necessarily representative of any operational structure.

2.2 Numerical model

The simulations have been performed using the multi-dimensional, nonlinear, structural-dynamics, continuum-analysis suite of codes, CTH [5] using a model very similar to that described in Ref. 1. Like Ref. 1, the simulations have used a three-dimensional, rectangular mesh; however, in this work, an assumed symmetry plane is not possible as there are potentially three-independent vectors when obliquity is allowed (velocity vector, shield normal and the cylinder, central axis).

The mesh is illustrated by the contour of the normalized mesh area in Fig. 2a. The mesh uses transverse rectangular cells measuring 0.3 mm in each direction (0.3 mm x 0.3 mm) with an area of 0.09 mm^2 in the central region that extends 1.5 cm from the impact location. Outside the central region, the mesh has been extended an additional 4.5 cm with a mesh size that increases linearly to 1.5 mm. The entire mesh in the through-thickness direction, as illustrated by a density contour in Fig. 2b, is discretized at a constant 0.3 mm such that the central region of the mesh is a cube of 0.3 mm dimensions. The mesh in the through-thickness direction extends 9 mm below the rear-wall and 5 mm or more above the outermost fabric to completely fit the projectile.

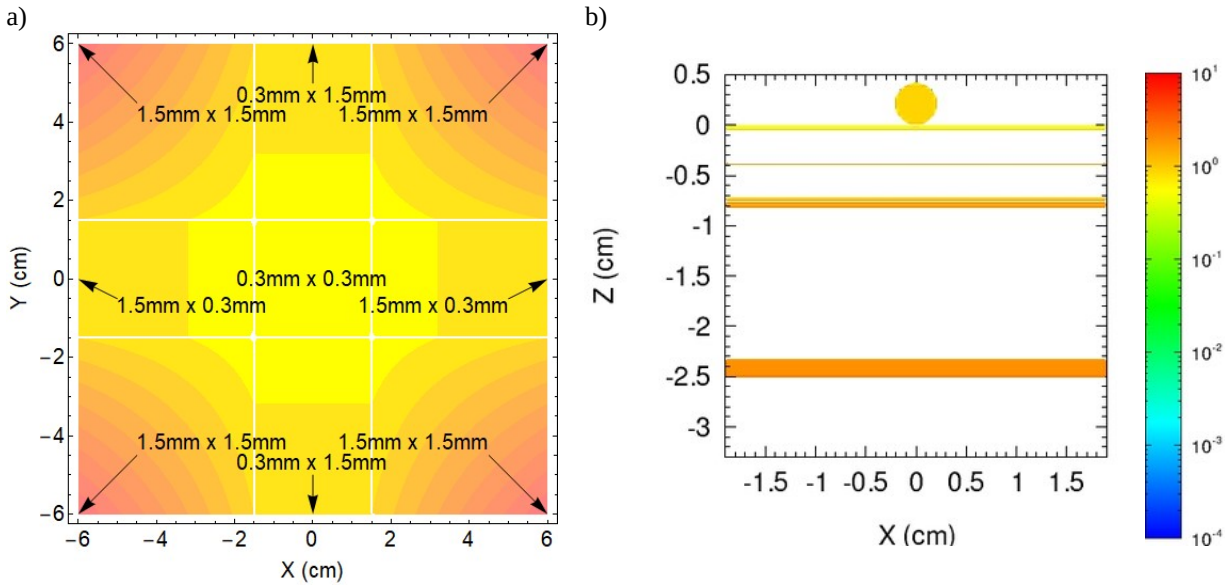

Fig. 2. Simulation space description with contours of the a) transverse mesh area with a 0.09 mm^2 minimum in the central region and 2.25 mm^2 maximum farthest from the center, and a representative b) density contour prior to impact of a spherical projectile. Contour in central region (0.3 mm x 0.3 mm x 0.3 mm).

The material models used are identical to those described in Ref. 3. Material is allowed to exit the mesh through all of the boundaries except the reflective boundary, and material is removed if its density falls below 10^{-5} g/cm^3 (a medium vacuum). In time, the simulations are performed to at least 35 μs after impact. If the rear wall continues to evolve, simulations are extended until the peak rear wall speed in the impact direction is less than a meter per second.

2.3 Numerical model validation

Recent impact experiments have been performed using cylindrical CFRP projectiles with length to diameter aspect ratios of approximately 1 to 5, 2 to 3 and 3 to 1 as illustrated in Fig. 3, 4 and 5, respectively [4]. The impact experiments were all approximately 7 km/s impacts and impacted normal to the shield of Fig. 1. In addition to the normal measurement of impact speed, detailed videography has been obtained to measure the orientation of the cylindrical projectiles at impact. Together these measurements of the necessary impact characteristics enabled comparison simulations of the impacts to validate the numerical model.

In each of the figures, pre-impact images of two different projectiles are shown. Along with the projectile images, post-impact, front-surface images of the aluminum rear wall are also shown. When this rear wall is penetrated, the projectile exceeds the ballistic limit of the shield, and when the rear wall remained intact, the projectile is less than the ballistic limit of the shield. In addition to the two experimental images, a density contour from the comparative simulation of the experiment are also shown.

In Fig. 3, the length to diameter of the cylindrical projectile is 1:5 in Fig. 3a and 1:2.5 in Fig. 3b. These projectiles are approximately flat disks. In both cases the length of the cylinder is 1.6 mm and the diameters are 8 mm and 4 mm in Fig. 3a and Fig. 3b, respectively, and as such, the mass of the projectile in Fig. 3a is twice that in Fig. 3b. As can be seen, the 1:5 projectile penetrated the shield rear wall, and the 1:2.5 projectile did not. The results from the

numerical model closely matches the findings from the experiments with a predicted penetration for the 1:5 and a cratered intact shield for the 1:2.5 projectile.

a)

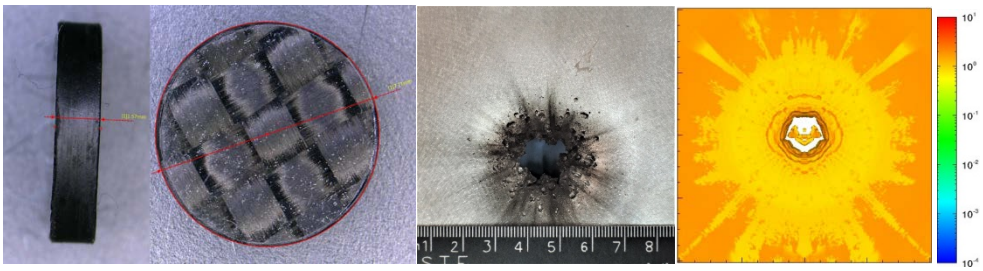

b)

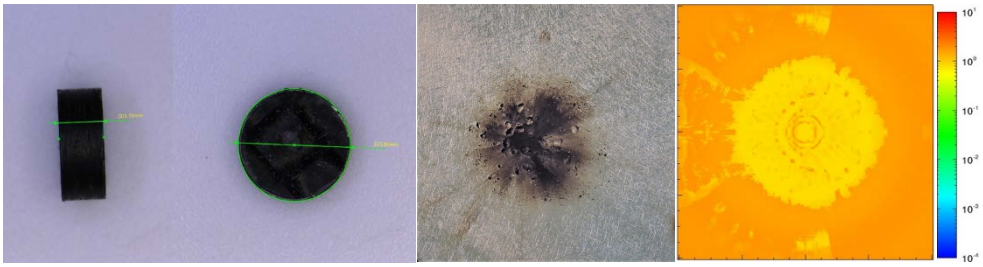

Fig. 3. Damage to the rear wall from CFRP projectiles a) 8.0 mm diameter and 1.6 mm thickness and b) 4.0 mm diameter and 1.6 mm thickness with comparative images. Tick marks in density contours are 5 mm apart.

In Fig. 4, the length to diameter of the cylindrical projectile is held constant at 2:3. This length to diameter is of equivalent mass to a spherical projectile at the same diameter. In Fig. 4a, the diameter is 5 mm, and the length is 3.33 mm. In Fig. 4b, the diameter is 3.45 mm, and the length is 2.3 mm. The 5 mm diameter projectile penetrated the shield rear wall, and the 3.45 mm projectile did not. The comparative agreement between the experiment and simulation is good.

a)

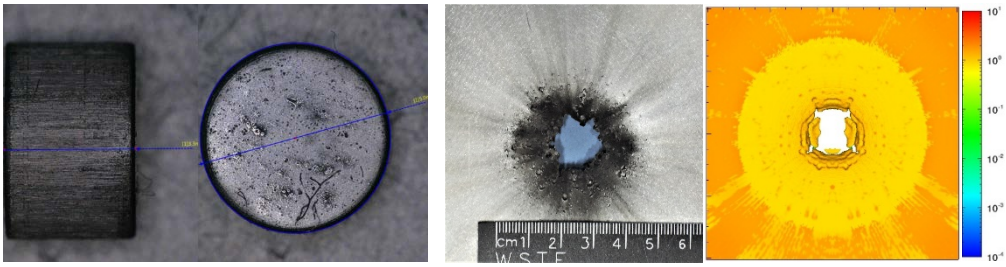

b)

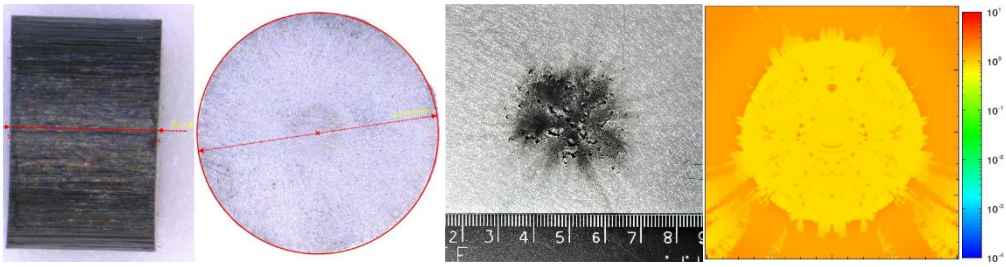

Fig. 4. Damage to the rear wall from CFRP projectiles a) 5.0 mm diameter and 3.33 mm thickness and b) 3.45 mm diameter and 2.3 mm thickness with comparative images. Tick marks in density contours are 5 mm apart.

In Fig. 5, the length to diameter of the cylindrical projectile is again held constant but at 3:1. In Fig. 5a, the diameter is 2.5 mm and the length is 7.5 mm, and in Fig. 5b, the diameter is 1.75 mm, and the length is 5.25 mm. As can be seen, the 2.5 mm diameter projectile produced a significant, linear crater and had sub-millimeter perforations in the

shield rear wall, and the 1.75 mm diameter projectile produced smaller more spherical craters. The results from the numerical model closely matches the findings from the experiments.

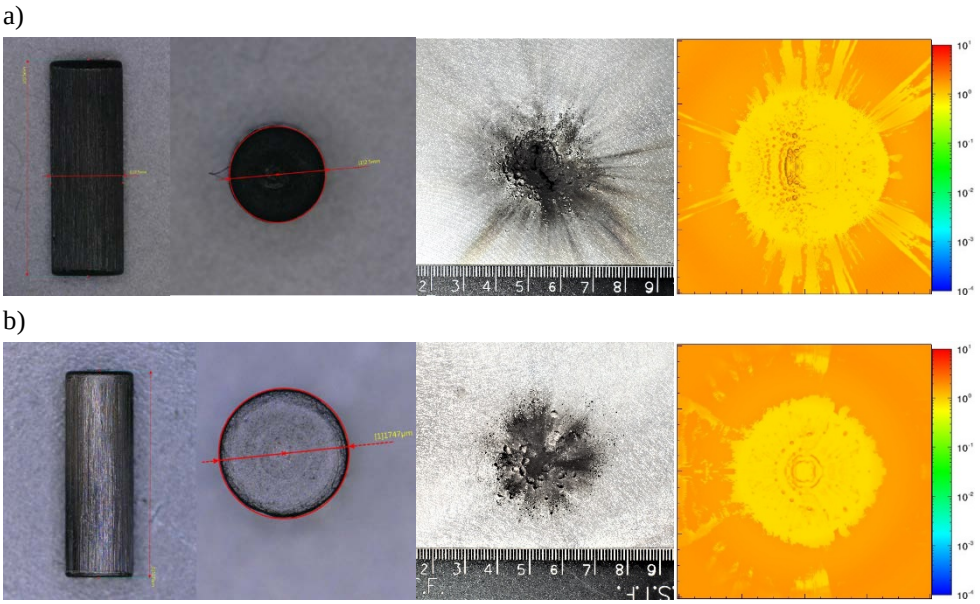

Fig. 5. Damage to the rear wall from CFRP projectiles a) 2.5 mm diameter and 7.5 mm thickness and b) 1.75 mm diameter and 5.25 mm thickness with comparative images. Tick marks in density contours are 5 mm apart

Although the development of techniques to obtain test results for cylindrical shaped CFRP projectiles is a significant development, the broad variation of impact conditions makes it essential to have robust numerical models to tightly control impact variables to see the effect of each variable over randomly obtained variation from test. As the comparisons of numerically obtained impact results and the experiments performed show good agreement, the numerical modeling has been used to extend these results to other conditions most notably obliquity (the projectile velocity vector is not collinear with the shield surface normal). The introduction of obliquity means that a favorable plane that contains both the projectiles axis of symmetry and the shield surface normal cannot necessarily be selected, which means that an additional two impact variables (pitch and yaw) are needed. This work addresses this consideration for this shield.

3 RESULTS

With the numerical model developed and validated to the limits of current capability, just under six hundred simulations using the assumed characteristics of CFRP projectiles impacting the shield have been performed to extend the numerical database to oblique impacts at 7 km/s. As the cylindrical impact condition does not necessarily have rotational symmetry about the axis orthogonal to the impact vector, the evaluation has considered two different conditions: the cylinder-axis is in the same plane as the velocity vector and the shield surface normal (only projectile pitch or attack-angle is necessary), and the cylinder-axis is outside the plane of the velocity vector and the shield surface normal (both projectile pitch and yaw are necessary).

3.1 Cylinder-axis in-plane

Approximately two-hundred and fifty simulations have been performed where the central axis of the projectile is in the same plane as the velocity vector and the shield surface normal. These simulations addressed four different obliquities evenly spaced at 22.5° from a normal impact at 0° to 67.5°. In this impact condition, a favorable plane can be selected and there is no need for yaw. These conditions are illustrated in Fig. 6 for four different pitch angles: 0° (cylinder axis is collinear with the velocity vector) shown in Fig. 6a, 90° (cylinder axis is orthogonal to the velocity vector) shown in Fig. 6b, +45° (cylinder axis rotated counterclockwise toward orthogonal) shown in Fig. 6c, and -45° (cylinder axis rotated clockwise toward orthogonal) shown in Fig. 6d.

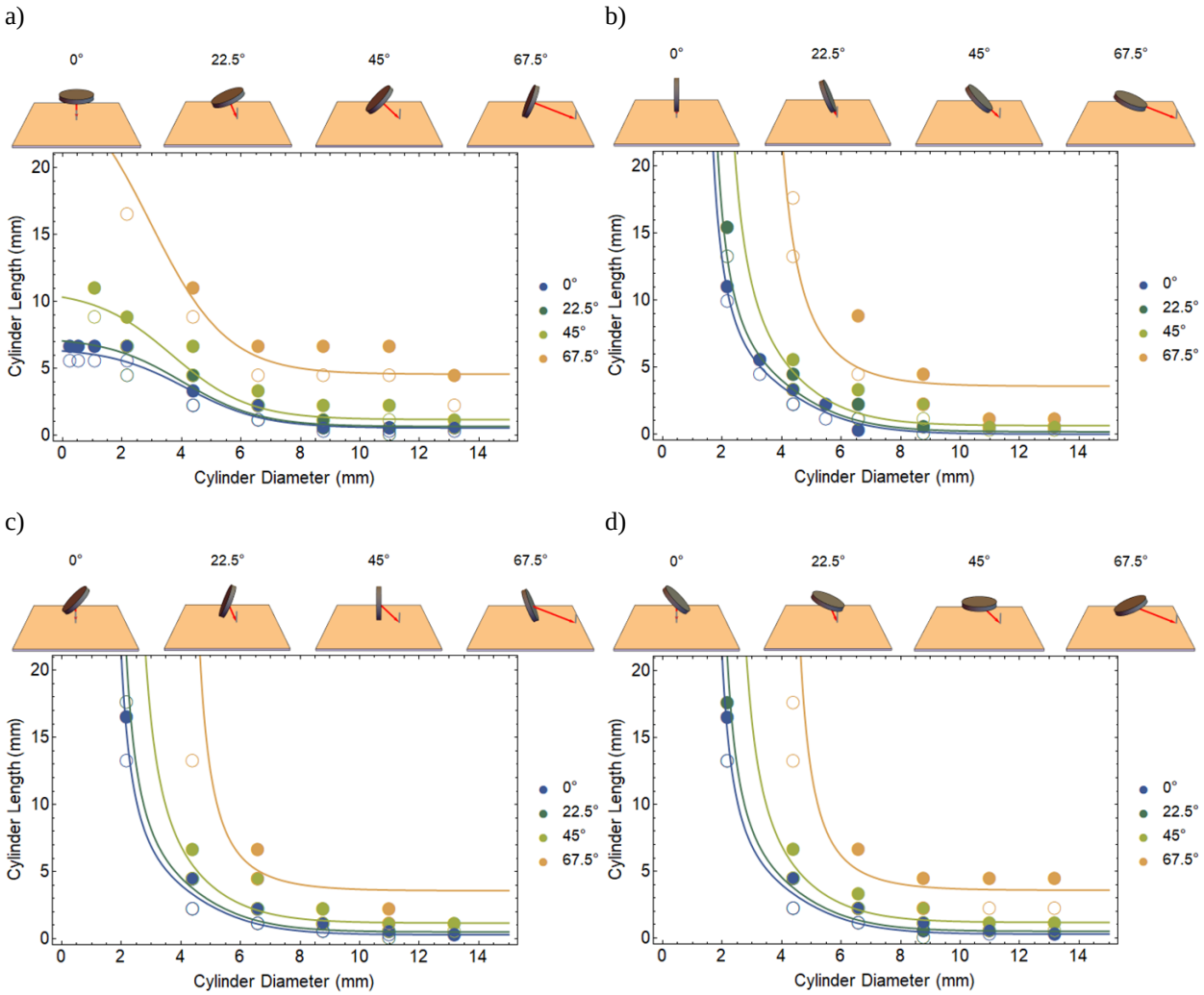

Fig. 6. Representative results of critical cylinder length against a Whipple shield as a function of cylinder diameter, obliquity and orientation. The orientation in a) is cylinder aligned with the velocity vector, b) is orthogonal to the velocity vector, c) rotated +45° from the velocity vector, and d) rotated -45° from the velocity vector. Shield results, shown by circles, are open for an intact shield and filled for a failed shield; along with the model as curves.

In addition to the illustrations of the impact conditions, Fig. 6 shows the simulation results as circles over the domain of cylinder lengths and diameters considered as data points. These simulation results are segregated by impact obliquity for each of the four obliquities considered and each of the pitch angles. In the figure, if the simulated rear wall is penetrated, the circle is shown filled and if the rear wall remains intact the circle is shown open. The transition from open to filled represents the ballistic limit of the shield for the given conditions.

A generalized model to define the ballistic limit of the shield is necessary to increase the utility of the observations. To this end, the collection of the transitions from intact to penetrated shields has been fit using a nonlinear regression for the critical cylinder length as a function of cylinder diameter, obliquity and pitch angle. The critical length is given by:

$$L_{Cyl}\left[D_{Cyl},\alpha,\theta\right] = \mathrm{Cos}[|\alpha|\,\theta]^{0.5}\left(0.496\mathrm{Cos}[|\alpha|]^2 + 3.043\left(1 - \mathrm{Tanh}\left[\frac{D_{Cyl}-4.132\,\mathrm{Sec}[\theta]^{1.154}}{2.679}\right]\right)\mathrm{Coth}\left[\frac{\left(D_{Cyl}+\mathrm{Cos}[^\circ q]^{6.215}\left(9.264-26.79\mathrm{Sin}[|\alpha|]+16.33\mathrm{Sin}[|\alpha|]^2\right)-4.273\,\mathrm{Sin}\left[\sqrt{|\alpha|\theta}\right]^{3.420}\right)}{1.944\,\mathrm{Sec}[\theta]^{1.209}}\right]\right) \quad (1)$$

where D_{Cyl} is the cylinder diameter in millimetres, α is the pitch angle and θ is the obliquity. This generalized model is shown as curves linked to the corresponding obliquity in Fig. 6 for each of the pitch angles considered numerically. These curves represent the critical geometric properties of the projectile at 7 km/s and requires the integration with the environment definition to further simplify for use in existing system reliability tools.

While the inclusion of both obliquity and pitch is significant, an additional impact variable is left out of this development. The constraint that the cylinder axis, the velocity vector and shield surface normal are all in the same plane is a significant simplification. To address this constraint, an additional impact variable that describes the rotation angle of the projectile's central axis away from that plane is needed.

3.2 Cylinder-axis out-of-plane

Approximately three-hundred and fifty simulations have been performed where the central axis of the projectile is outside the plane defined by the velocity vector and the shield surface normal. These simulations addressed two different obliquities from a normal impact: 22.5° (Fig. 7) and 45° (Fig. 8). Similar to the unyawed orientation discussed in the previous section, the pitch angle is varied evenly over 180°. These conditions are illustrated for the same four different pitch angles: 0° shown in Fig. 7a and Fig. 8a, 90° shown in Fig. 7b and Fig. 8b, +45° shown in Fig. 7c and Fig. 8c, and -45° shown in Fig. 7d and Fig. 8d.

The rotation out-of-plane has been done by rotating the cylindrical projectile about the surface normal by 22.5°, 67.5°, 112.5° and 157.5° from the velocity vector as illustrated in both Fig. 7 and Fig. 8. The results of the simulations, intact shields are shown as an open circle and penetrated shields are shown as filled circles. As a point of comparison, all of the data described in Section 3.1 is also shown with the yawed data presented in this section. The yawed data is plotted second; therefore, if the unyawed data is not visible it is because the critical geometry of the projectile is unaffected by the rotation outside of the plane of the velocity vector and the shield surface normal. As can be seen for both the 22.5° obliquity shown in Fig. 7 and the 45° obliquity shown in Fig. 8, the rotation outside of the plane defined by the velocity vector and the shield surface normal has a modest effect relative to the obliquity and the pitch of the projectile in flight, and as such, further development of the generalized fit from Eqn. 1 has not been performed.

4 DISCUSSION

Numerical models have been compared to experimental data and have shown that they reproduce those findings well. These validated numerical models have then been used to extrapolate from those conditions to a significantly expanded domain of impact variables. Specifically, the numerical models allow the fine control of impact conditions to determine the influence on the final performance of the shield; whereas, in experiment, these variables are not easily controlled and requires many tests to map out the effect. This numerical sweep has been performed in great detail for the shield described in Fig. 1.

Previous work [1] focused on the normal impacts into this shield where the pitch (angle-of-attack) of the cylindrical projectile was varied and a form of critical length was developed to describe the dependence on cylinder diameter and angle-of-attack. This work has been expanded here into the form of Eqn. 1, and Eqn. 1 collapses to the form of the critical length in Ref. 1 when the obliquity is taken to be 0° ($\theta = 0°$). As indicated in Eqn. 1, the critical length is now described by three independent parameters including the cylinder diameter, the pitch, and the obliquity. To illustrate how these variables affect the critical mass, a three dimensional density contour plot of the critical mass is shown in Fig. 9. In the figure, the mass of the critically dimensioned cylinder is normalized to the mass of the previously determined critical spherical projectile with a diameter of 4.3 mm [3] and assuming the traditional obliquity dependence of the Whipple shield for mass, $Cos^{-2}[\theta]$. When the critical cylinder has the same mass as the critical sphere, the ratio is unity, and in turn, when the critical cylinder is more massive than the sphere the ratio is greater than unity and less massive less than unity. To aid in interpreting this plot, when the critical cylinder mas is approximately the same as the critical spherical mass (critical mass ratios between 0.67 and 1.33), the data is transparent to allow focusing on the conditions where the performance is significantly different than that expected for a spherical projectile.

As can be seen in the figure, the critical mass of the cylindrical projectile can be greater for small diameter projectiles with high pitch and large diameter projectiles with small pitch. The opposite condition, where the critical mass of the cylindrical projectile is less than the spherical projectile, shows that small diameter projectiles with low pitch and large diameter with high pitch are critical to the shield.

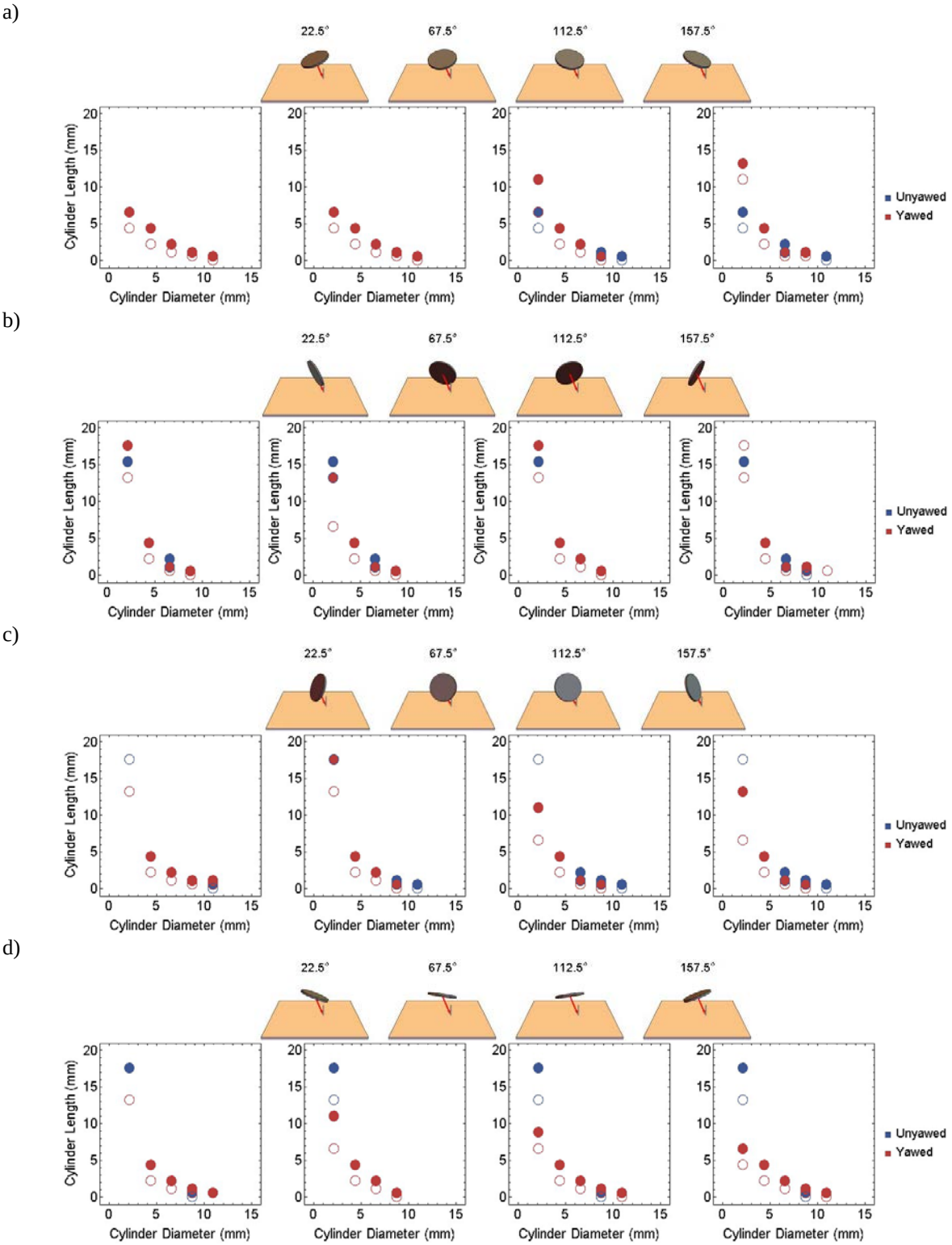

Fig. 7. Representative results of critical cylinder length for a 22.5° obliquity against a Whipple shield as a function of cylinder diameter and orientation. The orientation in a) is cylinder aligned with the velocity vector, b) is orthogonal to the velocity vector, c) rotated +45° from the velocity vector, and d) rotated -45° from the velocity vector. The projectiles are varied outside of the velocity vector and shield surface normal plane by 22.5°, 67.5°, 112.5° and 157.5°. Shield results, shown by circles, are open for an intact shield and filled for a failed shield; along with the model as curves.

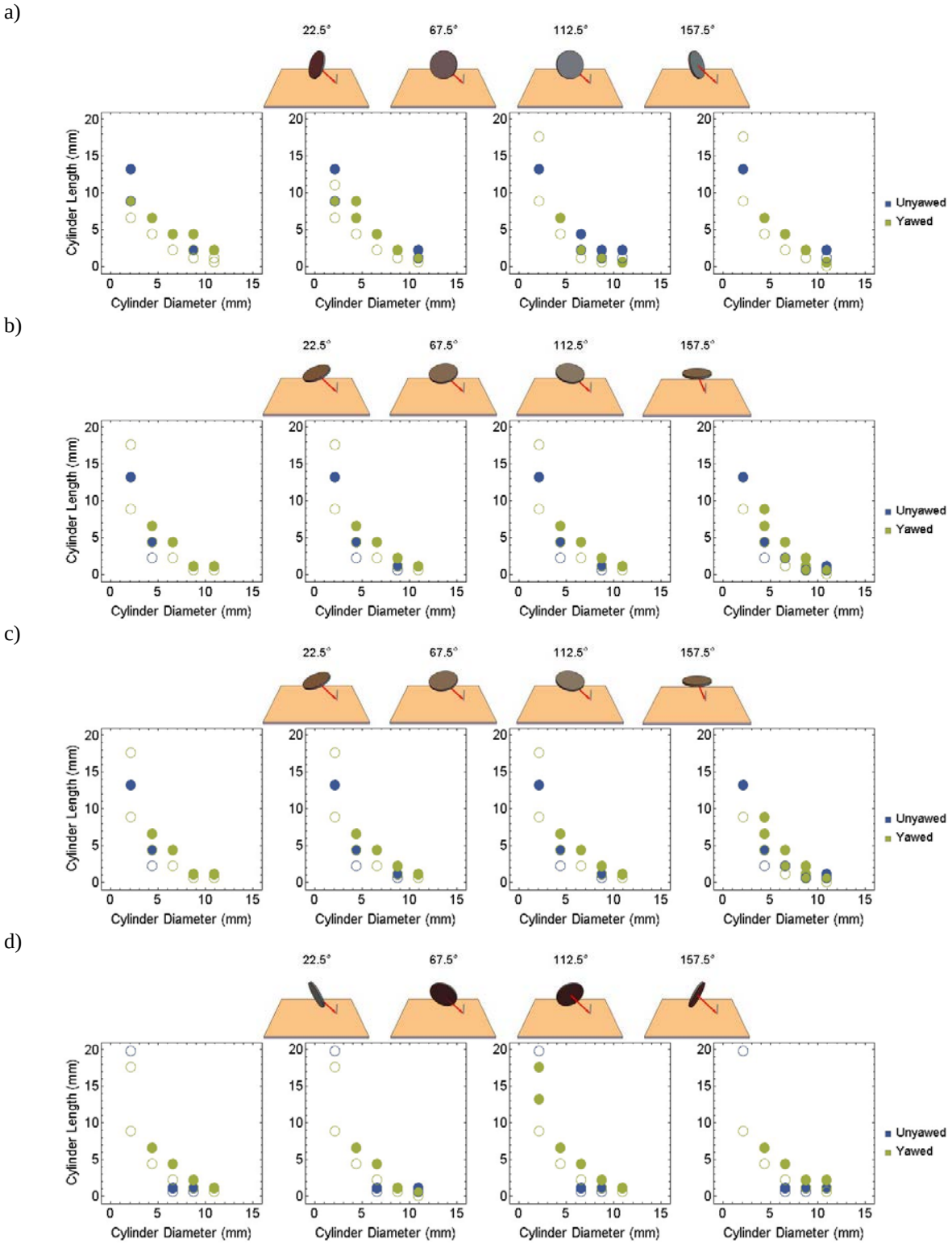

Fig. 8. Representative results of critical cylinder length for a 45° obliquity against a Whipple shield as a function of cylinder diameter and orientation. The orientation in a) is cylinder aligned with the velocity vector, b) is orthogonal to the velocity vector, c) rotated +45° from the velocity vector, and d) rotated -45° from the velocity vector. The projectiles are varied outside of the velocity vector and shield surface normal plane by 22.5°, 67.5°, 112.5° and 157.5°. Shield results, shown by circles, are open for an intact shield and filled for a failed shield; along with the model as curves.

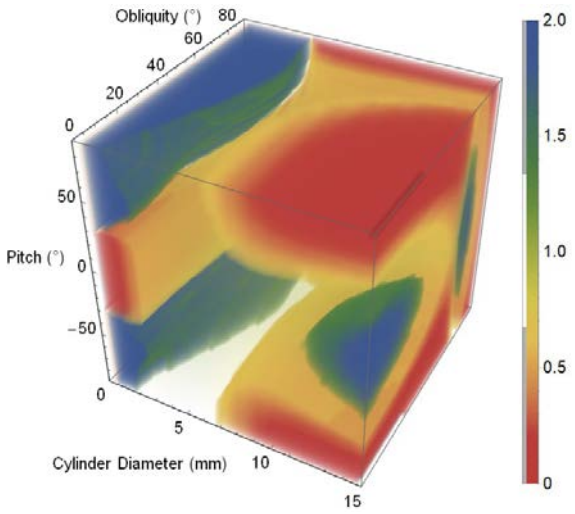

Fig. 9. Contour plot of the critical cylinder to sphere mass ratio for this shield. Ratio less than 1 means the critical cylinder is smaller than the critical sphere for this shield, and the ratio greater than 1 is the opposite.

5 CONCLUSION

The complicated nature of oblique impacts of cylindrical projectiles has been explored through numerical simulation for a common shield in a configuration of relevance to human spaceflight. This work is for a single impact speed and projectile material. The numerical model that has been developed for this effort has been validated against recently obtained experimental data for the shield and has shown good agreement between the simulations and the experiments. Using the model, a broad sweep of impact obliquities and projectile orientations has been performed. It has been found that the work of Ref. 3 can be extended to include impact obliquity when the angle-of-attack is taken to be the pitch of the projectile in flight. It was also found that yaw of the projectile, did have some dependence, the dependence is modest. Using these findings it has been found that the rod penetrators with little pitch and flat disk like penetrator with high pitch are of the highest concern. These findings should be integrated with environment models and extended with impact speed to make the final determination on the effect of non-spherical projectiles.

6 ACKNOWLEDGEMENTS

The author wishes to gratefully acknowledge the Jacobs JETS contract NNJ13HA01 in its support to the Hypervelocity Impact Technology group at NASA Johnson Space Center and its sponsorship to University of Texas at El Paso under EN41520TMS, and the White Sands Test Facility Remote Hypervelocity Impact Laboratory and the Hypervelocity Impact Technology test team for the seamless execution of the experimental work.

7 REFERENCES

1. Miller, J.E., “Simulation study of non-spherical, graphite-epoxy projectiles”, Proceedings of the 2019 Hypervelocity Impact Symposium, Destin, FL, HVIS2019-044 (2019).
2. Liou, J.-C., et. al., “DebriSat-A planned laboratory-based satellite impact experiment for breakup fragment characterization”, 6th European Conference on Space Debris at Darmstadt, Germany, ESA SP-723, 41 (2013).
3. Fitz-Coy, N., et. al., “Characterization of debris from the Debrisat hypervelocity test”, 66th International Astronautical Congress at Jerusalem, Israel, IAC-15-A6.2.9x30343, pp. 1-10 (2015).
4. McCandless, R.J., et. al., “OSMA CFRP Shape Effect HVI Research Program”, JSC Report #, (2019).
5. McGlaun, J., et. al., “CTH: a three-dimensional shock wave physics code”, Int. J. Impact Eng., 10, pp. 351-360 (1990).